

A series of $[\text{Na}_2\text{Mn}_2^{\text{II}}\text{Mn}_6^{\text{III}}]$ clusters derived from trigonal bipyramidal $[\text{NaMn}^{\text{II}}\text{Mn}_3^{\text{III}}]$ subunits bridged by mono-, di- and tri-fold azide groups: synthesis, crystal structures and magnetic properties

Jiang Liu, Quanling Suo, Jian Song, Lijuan Zhang, Yuanyuan Gao*

College of Chemical Engineering, Inner Mongolia University of Technology, Hohhot 010051, China

ARTICLE INFO

Article history:

Received 18 September 2018

Accepted 8 December 2018

Available online 18 December 2018

Keywords:

Coordination polymers

Decanuclear clusters

Crystal structure

Magnetic properties

Multidentate Schiff base ligands

ABSTRACT

A series of $[\text{Na}_2\text{Mn}_2^{\text{II}}\text{Mn}_6^{\text{III}}]$ clusters derived from trigonal bipyramidal $[\text{NaMn}^{\text{II}}\text{Mn}_3^{\text{III}}]$ subunits bridged by mono-, di- and tri- fold azide groups $\text{Na}[\text{Na}_2\text{Mn}_2^{\text{II}}\text{Mn}_6^{\text{III}}(\mu_3\text{-O})_2(\text{HL}^1)_6(\mu_{1,3}\text{-N}_3)(\text{HCOO})_8(\text{H}_2\text{O})_2](\text{ClO}_4)_2$ (**1**), $[\text{Na}_2\text{Mn}_2^{\text{II}}\text{Mn}_6^{\text{III}}(\mu_3\text{-O})_2(\text{L}^2)_6(\mu_{1,1}\text{-N}_3)_4(\mu_{1,3}\text{-N}_3)_2(\text{N}_3)_2(\text{CH}_3\text{OH})_2]$ (**2**) and $[\text{Na}_2\text{Mn}_2^{\text{II}}\text{Mn}_6^{\text{III}}(\mu_3\text{-O})_2(\text{L}^3)_6(\mu_{1,1}\text{-N}_3)_7(\text{N}_3)_2(\text{H}_2\text{O})_2]$ (**3**) have been obtained via the self-assembly of different potentially multidentate Schiff base ligands and auxiliary ligands (azide ions and formate ions) with divalent manganese salt in an air-exposed water-methanol solution. The structures of **1**, **2** and **3** were characterized by elemental analysis, FT-IR spectroscopy and single-crystal X-ray diffraction analysis. Crystal structures reveal that all the three similar interesting decanuclear clusters $[\text{Na}_2\text{Mn}_2^{\text{II}}\text{Mn}_6^{\text{III}}]$ are derived from double trigonal bipyramid subunits bridged by mono-, di- and tri- fold azide groups, respectively. The magnetic susceptibility studies of **1**, **2** and **3** in the temperature range 2–300 K shows that predominantly antiferromagnetic interactions between the manganese centers.

© 2018 Elsevier Ltd. All rights reserved.

1. Introduction

Over the past decades, the rational design and constructing new type of polynuclear clusters based on the assembly of multifunctional organic ligands and auxiliary bridged ligands with metal ions are increasingly interesting because of their intriguing structural diversities and potential applications. Polynuclear clusters with highly intriguing properties that render them attractive candidates for single-molecular magnets [1–3], ferroelectric materials [4–7], luminescent materials [5,8,9] and catalysis [10–12], and so on. Up to now, many kinds of polynuclear clusters have been reported such as 3d transition metal clusters and 3d–4f mixed metal clusters [13–15]. Among them, mixed-valence manganese clusters have been the research focus of coordination chemists due to their potential large ground spin state and magnetic anisotropy. So far, an increasing number of mixed-valence manganese polynuclear clusters presenting different nuclear number, versatile bridge mode, interesting topology structure and various bulk magnetic properties have been reported [13,16–20].

The multidentate Schiff base ligands are important in controlling the structure of clusters and have been extensively used in assembling of polynuclear clusters due to their facile synthesis

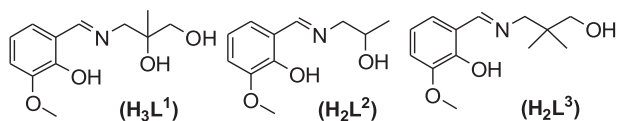
procedure, tunable steric properties, and good solubility. Additionally, introducing short bridging ligands such as the azide anion (N_3^-) and formate anion (HCOO^-), serving as auxiliary ligands, also play an important role in modulating skeleton structure of the polynuclear clusters. Indeed, the N_3^- anion has been widely used to generate coordination polymers owing to the versatile coordination modes of $\mu_{1,1}$ -(end-on, EO), $\mu_{1,3}$ -(end-to-end, EE) bridges [21–25]. Furthermore, the formate anion also can act as a triatomic bridging ligand in metal–organic complexes.

During our continuing efforts to construct polynuclear paramagnetic clusters, especially mixed-valence manganese clusters, we choose three similar multidentate Schiff base ligands (Scheme 1) together with azide anion and/or formate anion as auxiliary ligands to prepare polynuclear manganese clusters. The steric effects derived from different multidentate Schiff base ligands and the modulating roles of auxiliary ligands lead to the difference in the structures and magnetic properties of the clusters.

Herein, the synthesis, crystal structure of three mixed-valence polynuclear manganese clusters $\text{Na}[\text{Na}_2\text{Mn}_2^{\text{II}}\text{Mn}_6^{\text{III}}(\mu_3\text{-O})_2(\text{HL}^1)_6(\mu_{1,3}\text{-N}_3)(\text{HCOO})_8(\text{H}_2\text{O})_2](\text{ClO}_4)_2$ (**1**), $[\text{Na}_2\text{Mn}_2^{\text{II}}\text{Mn}_6^{\text{III}}(\mu_3\text{-O})_2(\text{L}^2)_6(\mu_{1,1}\text{-N}_3)_4(\mu_{1,3}\text{-N}_3)_2(\text{N}_3)_2(\text{CH}_3\text{OH})_2]$ (**2**) and $[\text{Na}_2\text{Mn}_2^{\text{II}}\text{Mn}_6^{\text{III}}(\mu_3\text{-O})_2(\text{L}^3)_6(\mu_{1,1}\text{-N}_3)_7(\text{N}_3)_2(\text{H}_2\text{O})_2]$ (**3**) have been synthesized. It should be noticed that these three clusters contains similar interesting double trigonal bipyramid subunits bridged by mono-, di- and tri- fold azide groups,

* Corresponding author.

E-mail address: gaoyuanyuan@imut.edu.cn (Y. Gao).



Scheme 1. Structural diagram of the multidentate Schiff base ligands.

respectively. And the magnetic properties of the three clusters have been explored.

2. Experimental

2.1. Materials and physical measurements

Caution! Although no problems were encountered during the preparation of the clusters, as sodium azide and perchlorate salts are potentially explosive, these basic materials should be treated with caution and used in small quantities.

All the starting chemicals and solvents were of AR grade and used as received. C, H and N analysis was carried out with a Perkin-Elmer 2400 elemental analyzer. The Fourier transform infrared spectra were recorded in the range of 4000–400 cm^{-1} using pressed KBr tablets on a MAGNA-IR750 type FT-IR spectrometer. Magnetic measurements between 2 and 300 K were carried out with a Quantum Design SQUID MPMS-7 magnetometer under a constant magnetic field of 1 kOe. Data were corrected for a capsule sample holder as well as for diamagnetic contributions.

2.2. Preparation of Schiff base ligands and complexes 1–3

H_3L^1 , H_2L^2 and H_2L^3 Schiff base ligands were prepared as described elsewhere in literature by a condensation reaction between 2-hydroxy-3-methoxybenzaldehyde and the corresponding amino alcohol (2-amino-2-methyl-1,3-propanediol, 1-amino-2-propanol, and 2-amino-2-methyl-1-propanol, respectively) under refluxing in the methanol solution. The resulting orange yellow solution containing the required product was used without further purification.

2.2.1. $\text{Na}[\text{Na}_2\text{Mn}_2^{\text{II}}\text{Mn}_6^{\text{III}}(\mu_3\text{-O})_2(\text{HL}^1)_6(\mu_{1,3}\text{-N}_3)(\text{HCOO})_8(\text{H}_2\text{O})_2](\text{ClO}_4)_2$ (**1**)

A mixture of H_3L^1 (1 mmol) and NaOH (0.2 mmol) in methanol-water (10/10 mL) was stirred for 30 min at room temperature. Then $\text{Mn}(\text{ClO}_4)_2 \cdot 6\text{H}_2\text{O}$ (1 mmol) were added to the above solution and stirred for further an hour. Finally HCOONa (1.5 mmol) and NaN_3 (0.5 mmol) were added and the solution was stirred for 1 hour under aerobic conditions. The resulting deep brown solution was filtered off and allowed to evaporate slowly in air. Dark brown bulk crystals were obtained after 7 days. Yield: 57% based on Mn (ClO_4)₂·6H₂O. Elemental Anal. Calc. for **1** ($\text{C}_{80}\text{H}_{104}\text{Mn}_8\text{N}_9\text{Na}_3\text{O}_{52}\text{Cl}_2$): C, 39.00; H, 4.28; N, 5.25. Found: C, 39.69; H, 4.13; N, 4.95%. FT-IR (cm^{-1}) for **1**: 3422m, 2909m, 2091m, 2057s, 1620s, 1586m, 1436m, 1307w, 1238w, 1095w, 741m, 624w.

2.2.2. $[\text{Na}_2\text{Mn}_2^{\text{II}}\text{Mn}_6^{\text{III}}(\mu_3\text{-O})_2(\text{L}^2)_6(\mu_{1,1}\text{-N}_3)_4(\mu_{1,3}\text{-N}_3)_2(\text{N}_3)_2(\text{CH}_3\text{OH})_2]$ (**2**)

A mixture of H_2L^2 (1 mmol) and NaOH (0.2 mmol) in methanol-water (10/10 mL) was stirred for 30 min at room temperature. Then $\text{Mn}(\text{ClO}_4)_2 \cdot 6\text{H}_2\text{O}$ (1 mmol) were added to the above solution and stirred for further an hour. Finally NaN_3 (0.5 mmol) was added and the solution was stirred for 1 h under aerobic conditions. The resulting deep brown solution was filtered off and allowed to evaporate slowly in air. Dark brown bulk crystals were obtained after 7 days. Yield: 52% based on $\text{Mn}(\text{ClO}_4)_2 \cdot 6\text{H}_2\text{O}$. Elemental Anal. Calc. for **2** ($\text{C}_{68}\text{H}_{74}\text{Mn}_8\text{N}_{30}\text{Na}_2\text{O}_{22}$): C, 37.90; H, 3.74; N, 19.50%. Found: C, 38.31; H, 3.51; N, 19.09%. FT-IR (cm^{-1}) for **2**: 3426m, 2921m,

2083m, 2060m, 1622s, 1589s, 1437m, 1306m, 1235w, 1092w, 742m, 624w.

2.2.3. $[\text{Na}_2\text{Mn}_2^{\text{II}}\text{Mn}_6^{\text{III}}(\mu_3\text{-O})_2(\text{L}^3)_6(\mu_{1,1}\text{-N}_3)_7(\text{N}_3)_2(\text{H}_2\text{O})_2]$ (**3**)

A mixture of H_2L^3 (1 mmol) and NaOH (0.2 mmol) in methanol-water (10/10 mL) was stirred for 30 min at room temperature. Then $\text{Mn}(\text{ClO}_4)_2 \cdot 6\text{H}_2\text{O}$ (1 mmol) were added to the above solution and stirred for further an hour. Finally NaN_3 (0.5 mmol) was added and the solution was stirred for 1 hour under aerobic conditions. The resulting deep brown solution was filtered off and allowed to evaporate slowly in air. Dark brown bulk crystals were obtained after 7 days. Yield: 52% based on $\text{Mn}(\text{ClO}_4)_2 \cdot 6\text{H}_2\text{O}$. Elemental Anal. Calc. for **3** ($\text{C}_{78}\text{H}_{106}\text{Mn}_8\text{N}_{33}\text{Na}_2\text{O}_{22}$): C, 39.59; H, 4.51; N, 19.53%. Found: C, 40.05; H, 4.79; N, 19.96%. FT-IR (cm^{-1}) for **3**: 3422m, 2933m, 2067s, 1612m, 1444m, 1302w, 1223w, 1089w, 750w, 619w.

2.3. X-ray crystallography

X-ray crystallography measurements for **1–3** were determined at 293(2) K on Rigaku Saturn724+ and Bruker Apex II CCD diffractometer with Mo K α radiation ($\lambda = 0.71073$ Å) operating in a ω -2 θ scanning mode for the data collection. The suitable structures of them were both solved by direct methods and refined anisotropically by full-matrix least squares techniques on F^2 values, using the SHELX-97 program [26,27]. Hydrogen atoms were added at appropriate theoretical positions and refined with isotropic thermal parameters riding on those parent atoms. The corresponding crystallographic and refinement data for **1–3** listed in Table 1.

3. Results and discussion

Complexes **1–3** were readily obtained by the reaction of a divalent manganese salt with the multidentate Schiff-base ligands H_3L^1 , H_2L^2 , H_2L^3 (Scheme 1) which are formed by the in situ condensation of o-vanillin with the corresponding amino alcohol, and in the presence of NaOH and auxiliary ligands sodium formate or sodium azide. During the reaction, the Mn^{II} ions is partially oxidized to the Mn^{III} ions in the open air. Dark brown single crystals of **1–3** suitable for X-ray analysis were obtained by slow evaporation at room temperature. The results of single crystal structure analysis indicate that when the formate and azide anion serves as the auxiliary ligand in the self-assembling procedure, a polynuclear cluster **1** which contains mono-azide group bridging trigonal bipyramid subunits was formed. While, di- and tri- fold azide groups bridged trigonal bipyramid complexes of **2** and **3** were obtained only using the azide anion as auxiliary ligand.

3.1. Description of crystal structures

3.1.1. Crystal structure of **1**

Single-crystal X-ray diffraction analyses reveal that complex **1** crystallizes in the triclinic space group P1. The coordination environment of **1** is depicted in Fig. 1(a) and the skeleton structure for the cluster is shown in Fig. 1(b). The skeleton structure of complex **1** consists of two perfectly symmetrical double trigonal bipyramid units ($[\text{NaMn}^{\text{II}}\text{Mn}_3^{\text{III}}]$ cluster) bridged by one μ -1,3 (end-to-end) azide. In detail, the core of each subunit contains one Mn^{II} , three Mn^{III} , one Na^{I} ions and three Schiff base ligands (H_3L^1). Each of the ligands coordinates to three metal ions (Mn^{II} , Mn^{III} and Na^{I}) along the blade of the propeller-shaped molecule. Three six-coordinated Mn^{III} ($\text{Mn}1$, $\text{Mn}2$, $\text{Mn}3$) ions are linked to each other via μ_3 -O bridge forming the planar $[\text{Mn}_3^{\text{III}}\text{O}]$ moiety and further connected by one $\mu_{1,3}$ -HCOO and two $\mu_{1,1}$ -HCOO bridges. Then one Na^{I} ion and one Mn^{II} ion is linked to the triangle plane by three Schiff base

Table 1
Crystal data and structure refinement for complexes 1–3.

| | 1 | 2 | 3 |
|---|---|---|--|
| Formula | C ₈₀ H ₁₀₄ Mn ₈ N ₉ Na ₃ O ₅₂ Cl ₂ | C ₆₈ H ₇₄ Mn ₈ N ₃₀ Na ₂ O ₂₂ | C ₇₈ H ₁₀₆ Mn ₈ N ₃₃ Na ₂ O ₂₂ |
| Mr | 2603.12 | 2149.08 | 2343.46 |
| Crystal system | triclinic | monoclinic | monoclinic |
| Space group | $P\bar{1}$ | $P2(1)/c$ | $P2(1)/m$ |
| <i>a</i> (Å) | 13.074(3) | 19.1307(1) | 12.393(3) |
| <i>b</i> (Å) | 13.156(3) | 11.7131(7) | 35.557(7) |
| <i>c</i> (Å) | 15.854(3) | 25.1793(1) | 13.123(3) |
| α (°) | 93.08(3) | 90 | 90 |
| β (°) | 95.86(3) | 128.921(3) | 115.44(3) |
| γ (°) | 90.82(3) | 90 | 90 |
| <i>V</i> (Å ³) | 2708.2(1) | 4389.7(4) | 5222.0(1) |
| <i>Z</i> | 1 | 2 | 2 |
| <i>T</i> (K) | 293(2) | 293(2) | 293(2) |
| <i>D</i> _{calc} (g cm ⁻³) | 1.596 | 1.626 | 1.490 |
| μ (mm ⁻¹) | 1.060 | 1.208 | 1.023 |
| <i>F</i> (0 0 0) | 1330.0 | 2180 | 2406 |
| θ range (°) | 1.56–25.01 | 1.37–25.02 | 1.15–25.01 |
| Reflections collected | 18 411 | 21 616 | 33 114 |
| Unique reflections | 9379 | 7730 | 9332 |
| <i>R</i> _{int} | 0.0455 | 0.0307 | 0.0697 |
| Goodness-of-fit (GOF) on <i>F</i> ² | 1.082 | 1.041 | 1.148 |
| <i>R</i> ₁ / <i>wR</i> ₂ [<i>I</i> > 2σ(<i>I</i>)] | 0.0963, 0.2872 | 0.0506, 0.1340 | 0.1142, 0.2905 |
| <i>R</i> ₁ / <i>wR</i> ₂ (all data) | 0.1133, 0.3039 | 0.0715, 0.1538 | 0.1519, 0.3211 |

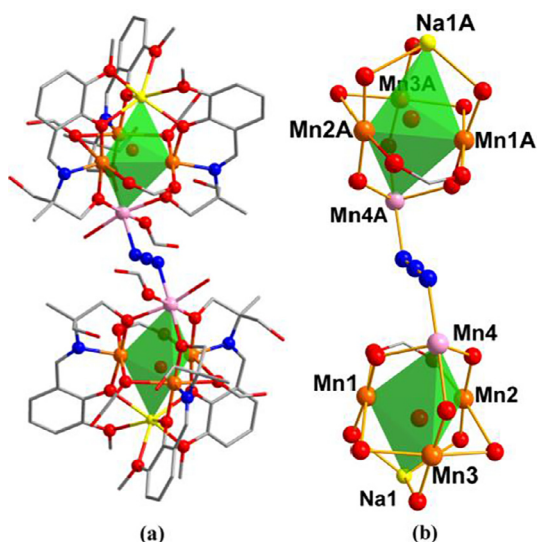


Fig. 1. Views showing (a) polyhedral representation of the structure of complex 1, (b) the skeleton structure for the core.

ligands (H_3L^1) separately. From the magnetic points of view, four paramagnetic metal ions in each subunit can be described as a super tetrahedron in which Mn^{II} ion acts as apex and $[Mn_3^{III}O]$ is the triangle plane. As a whole, two symmetrical double trigonal bipyramid subunits bridged by one $\mu_{1,3}$ - N_3 (end-to-end) azides via connecting the Mn^{II} apices.

In cluster 1, each of the three Schiff base ligands provides four different coordination sites from one deprotonated phenol O, one deprotonated hydroxyl O, imino N and methoxy O while another oxygen atom of hydroxyl is not involved in the coordination. All Mn^{III} ions are six-coordinated with distorted octahedral geometries. Among them, the coordination sites of Mn1 are occupied by phenolate oxygen, hydroxyl oxygen and imino nitrogen from one Schiff-base ligand, oxygen of μ_{3-O} bridge and two formic oxygen atoms. The coordination environments of Mn2 and Mn3 ions are the same as those in Mn1. The Mn^{II} (Mn4) ion assumes a distorted octahedral coordination geometry, which is completed by three

deprotonated hydroxyl oxygen atoms, a formic oxygen atom, a water oxygen atom and a nitrogen atom of azide. The Na^I ion above the $[Mn_3^{III}O]$ plane is six-coordinated by three oxygens of the deprotonated hydroxyls and three oxygens of the methoxys from three Schiff-base ligands. The selected bond lengths and angles for complex 1 are given in Table S1. The valences of the manganese metal ions are confirmed by bond-valence sum (BVS) calculations, which are listed in Table S4.

3.1.2. Crystal structures of 2

According to X-ray crystallographic analysis, complex 2 crystallizes in the monoclinic space group $P2_1/c$. The structure of 2 has been previously reported in literature [28]. As shown in Fig. 2, the skeleton structure of complex 2 consists of two perfectly symmetrical double trigonal bipyramid units bridged by two μ -1,3 (end-to-end) azide. In detail, the core of each subunit contains one Mn^{II} , three Mn^{III} , and one Na^I ions, which has similar trigonal bipyramid skeleton structure as in complex 1. The coordination environments of each metal ions are similar as that of in complex 1. In each of the trigonal bipyramid subunit ($[NaMn^{II}Mn_3^{III}]$), three deprotonated Schiff base ligands (H_2L^2) coordinate to metal ions

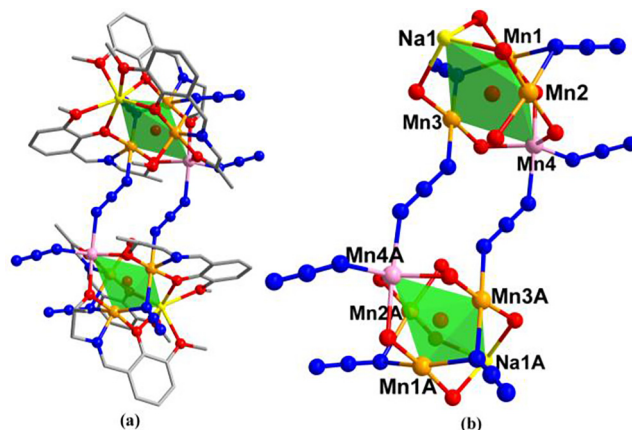


Fig. 2. Views showing (a) polyhedral representation of the structure of complex 2, (b) the skeleton structure for the core.

(Mn^{II}, Mn^{III} and Na^I) along the blade of the propeller-shaped molecule. Three six-coordinated Mn^{III} (Mn1, Mn2, Mn3) ions are linked to each other via μ_3 -O bridge forming the planar [Mn₃^{III}O] moiety. In this planar [Mn₃^{III}O] moiety, Mn1··Mn2 and Mn1··Mn3 are further connected by one $\mu_{1,1}$ -N₃ bridges, respectively. As it is described in complex **1**, one Na^I ion and one Mn^{II} (Mn4) ion is linked to the triangle plane forming a trigonal bipyramid subunit [NaMn^{II}Mn₃^{III}]. From the magnetic points of view, four paramagnetic metal ions in the subunit can be described as a super tetrahedron in which Mn^{II} ion acts as apex and [Mn₃^{III}O] is the triangle plane. Overall, two symmetrical double trigonal bipyramid subunits bridged by two $\mu_{1,3}$ -N₃ (end-to-end) azides via connecting Mn^{II}··Mn^{III} edges. The selected bond lengths and angles for complex **2** are given in Table S2. The valences of the manganese metal ions are confirmed by bond-valence sum (BVS) calculations, which are listed in Table S5.

3.1.3. Crystal structures of **3**

Complex **3** crystallizes in the monoclinic space group *P2₁/m*. The selected bond lengths and angles for complex **3** are shown in Table S1. The skeleton structure of complex **3** is shown as Fig. 3. The complex **3** consists of two perfectly symmetrical double trigonal bipyramid subunits bridged by three $\mu_{1,1}$ -N₃ (end-on) azides which adopt a different bridging mode from that of complex **1** or **2**. In complex **3**, the core of each subunit contains one Mn^{II}, three Mn^{III}, and one Na^I ions, which has similar trigonal bipyramid skeleton structure as in complex **1** and **2**. The coordination environments of each metal ion are similar as that of in complex **1** and **2**. In each of the trigonal bipyramid subunit ([NaMn^{II}Mn₃^{III}]), three deprotonated Schiff base ligands (H₂L³) coordinate to metal ions (Mn^{II}, Mn^{III} and Na^I) along the blade of the propeller-shaped molecule. Three six-coordinated Mn^{III} (Mn1, Mn2 and Mn4) ions are linked to each other via μ_3 -O bridge forming the planar [Mn₃^{III}O] moiety. In this planar [Mn₃^{III}O] moiety, Mn1··Mn2 and Mn1··Mn4 are further connected by one $\mu_{1,1}$ -N₃ bridges, respectively. As it is described in complex **1** and **2**, one Na^I ion and one Mn^{II} (Mn3) ion is linked to the triangle plane forming a trigonal bipyramid subunit [NaMn^{II}Mn₃^{III}]. From the magnetic points of view, four paramagnetic metal ions in the subunit can be described as a super tetrahedron in which Mn^{II} ion acts as apex and [Mn₃^{III}O] is the triangle plane. On the whole, two symmetrical double trigonal bipyramid subunits bridged by three $\mu_{1,1}$ -N₃ (end-on) azides via connecting Mn^{II} apex. The

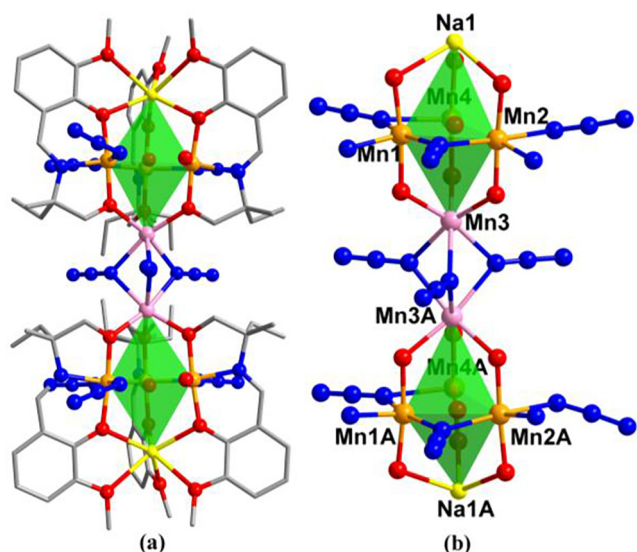


Fig. 3. Views showing (a) polyhedral representation of the structure of complex **3**, (b) the skeleton structure for the core.

selected bond lengths and angles for complex **3** are given in Table S3. The valences of the manganese metal ions are confirmed by bond-valence sum (BVS) calculations, which are listed in Table S6.

3.2. Magnetic properties

The magnetic properties of complexes **1–3** were studied to evaluate the magnetic interactions between the four paramagnetic centers. Variable temperature magnetic susceptibility measurements between 2 and 300 K under a constant magnetic field of 1 kOe were carried out.

The magnetic properties of **1–3** as a $\chi_M T$ against T plot are shown in Figs. 4–6. The room temperature $\chi_M T$ value is 20.35 cm³ K mol⁻¹ for **1**, 20.42 cm³ K mol⁻¹ for **2** and 21.56 cm³ K mol⁻¹ for **3**, much lower than the spin-only ($g = 2$) value of 26.75 cm³ K mol⁻¹ for the six Mn^{III} and two non interacting Mn^{II} ions. Upon cooling, the $\chi_M T$ decreases continuously in both cases indicating significant antiferromagnetic interactions between the magnetic centers. The rapid decrease for the three complexes the lower temperature can be due to intermolecular interactions and/or effects of zero-field splitting. According to the results of the single crystal structure analysis, combining with a magnetic point of view, the magnetic behaviors of **1** and **3** should mainly depend on the double-tetrahedron with Mn^{II} (Mn4) at the vertex and Mn^{III} (Mn1–Mn3) cations in the triangular plane. Thus, we can use the four- J isotropic Heisenberg model to evaluate the coupling interactions among the spin carriers within **1** and **3** [29]. The exchange interaction models can be represented as shown in the inset of Figs. 4 and 5, and the corresponding spin Hamiltonian is:

$$\hat{H} = -2J_1\hat{S}_4\hat{S}_5 - 2J_2(\hat{S}_4\hat{S}_1 + \hat{S}_4\hat{S}_2 + \hat{S}_4\hat{S}_3 + \hat{S}_5\hat{S}_6 + \hat{S}_5\hat{S}_7 + \hat{S}_5\hat{S}_8) \\ - 2J_3(\hat{S}_2\hat{S}_3 + \hat{S}_6\hat{S}_7) - 2J_4(\hat{S}_1\hat{S}_2 + \hat{S}_1\hat{S}_3 + \hat{S}_7\hat{S}_8 + \hat{S}_6\hat{S}_8)$$

For complex **1**, the MAGPACK simulation resulted in the best-fit parameters of $J_1 = -4.32$ cm⁻¹, $J_2 = -1.81$ cm⁻¹, $J_3 = -10.99$ cm⁻¹, $J_4 = -9.20$ cm⁻¹, $g = 2.03$. The negative value of J_1 represents antiferromagnetic coupling between the Mn^{II} (Mn4) ion, and the small negative J_2 value indicates antiferromagnetic interaction between the Mn^{II} (Mn4) and Mn^{III} (Mn1, Mn2 and Mn3) ions. J_3 represents antiferromagnetic interaction between the Mn1 and Mn2 ions. J_4 represents antiferromagnetic interaction between the Mn1 and Mn3 ions or between the Mn2 and Mn3 ions. For complex **3**, the MAGPACK simulation resulted in the best-fit parameters of $J_1 = -9.15$ cm⁻¹, $J_2 = -1.41$ cm⁻¹, $J_3 = -1.76$ cm⁻¹, $J_4 = -0.48$ cm⁻¹,

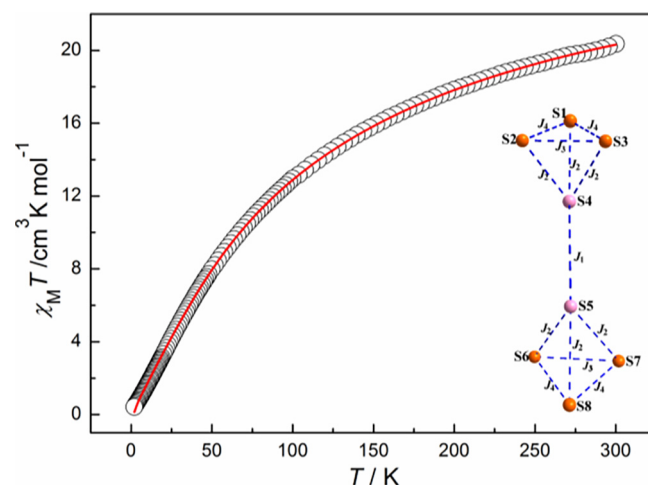


Fig. 4. Temperature dependence of the $\chi_M T$ for **1**, the solid line represents a simulation of the data as a best fit. Inset: The exchange interaction model used for **1**.

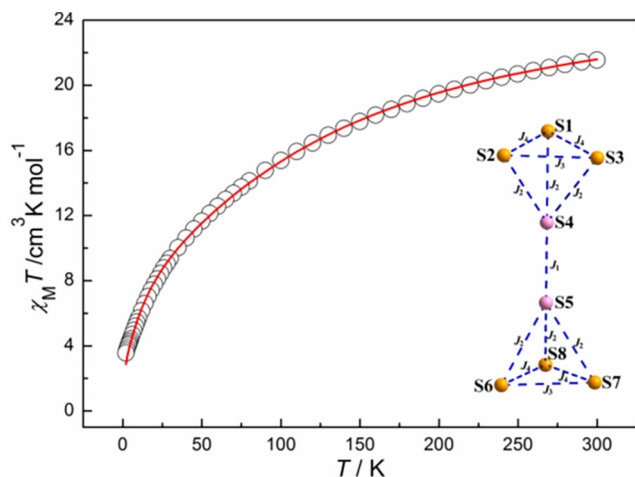


Fig. 5. Temperature dependence of the $\chi_M T$ for **3**, the solid line represents a simulation of the data as a best fit. Inset: The exchange interaction model used for **3**.

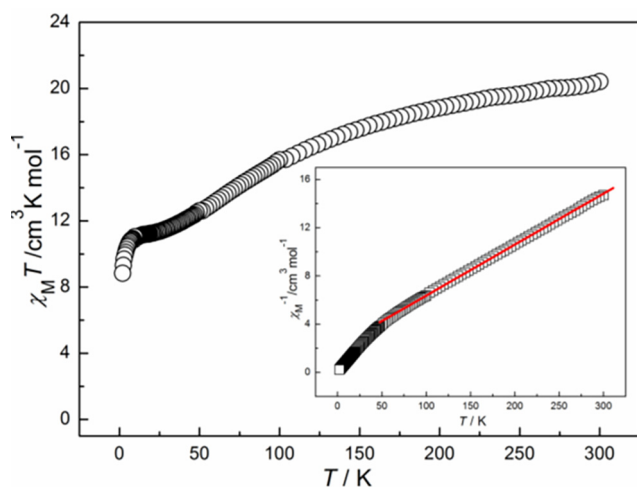


Fig. 6. Temperature dependence of the $\chi_M T$ and χ_M^{-1} (inset) for **2**. The solid line represents the fitted curve according to the Curie-Weiss law.

$g = 2.01$. The negative values of J_1 and J_2 represent antiferromagnetic interaction coupling of $\text{Mn}^{\text{II}} \cdots \text{Mn}^{\text{II}}$ and $\text{Mn}^{\text{II}} \cdots \text{Mn}^{\text{III}}$. J_3 and J_4 represent antiferromagnetic interaction coupling of $\text{Mn}^{\text{III}} \cdots \text{Mn}^{\text{III}}$. According to this previous literature, the magnetic properties of those reported complexes were mainly associated with their crystallographic condition, magnetic orbitals of spin centers (Mn ions), bond distances (Mn \cdots Mn) and angles (Mn–O–Mn and Mn–N (azido)–Mn) [30–33]. Based on theoretical predictions and experimental studies, the crossover angle from antiferromagnetic to ferromagnetic interactions of the end-on azido-bridges Mn(II) complexes is predicted to be 98° [33]. The general pattern presents an antiferromagnetic interaction with a bridging Mn(II)–N(azido)–Mn(II) bond angle of less than 98° . According to the literature, it may be reasonable that the Mn(II)–N(azido)–Mn(II) bond angles of **1** and **3** less than 98° producing values of $J_1 < 0$ (antiferromagnetic interaction). For **2**, because of the topological complexity of the molecule, it is not possible to determine the individual pairwise Mn ions exchange interactions using the Heisenberg method. The inverse magnetic susceptibilities curve shows a linear behavior in 50–300 K range and obeys the Curie-Weiss law, with $C = 23.62 \text{ cm}^3 \text{ K mol}^{-1}$ and $\theta = -50.44 \text{ K}$. The negative θ value indicates antiferromagnetic interaction between Mn ions.

4. Conclusions

In summary, a series of $[\text{Na}_2\text{Mn}^{\text{II}}\text{Mn}^{\text{III}}]$ clusters (**1–3**) have been obtained via the self-assembly by using different potentially multi-dentate Schiff base ligands and auxiliary ligands (azide ions and formate ions) with Mn(II) ions. The structural diversity of three coordination compounds indicates that the structures can be tuned by modification of Schiff base ligands. Based upon the structural features, the temperature dependence of magnetic susceptibility of complexes **1** and **3** was modeled with MAGPACK using isotropic Heisenberg Hamiltonians. The magnetic coupling parameters have been evaluated and the results indicate that there exist antiferromagnetic interactions between the magnetic centers.

Acknowledgments

This work was supported by the National Natural Science Foundation of China (21761026) and the Natural Science Foundation of Inner Mongolia (2016BS0206).

Appendix A. Supplementary data

CCDC 1854652, 1854653 and 1854654 contains the supplementary crystallographic data for **1–3**, respectively. These data can be obtained free of charge via <http://www.ccdc.cam.ac.uk/conts/retrieving.html>, or from the Cambridge Crystallographic Data Centre, 12 Union Road, Cambridge CB2 1EZ, UK; fax: (+44) 1223-336-033; or e-mail: deposit@ccdc.cam.ac.uk. Supplementary data to this article can be found online at <https://doi.org/10.1016/j.poly.2018.12.007>.

References

- [1] G.J. Halder, C.J. Kepert, B. Moubaraki, K.S. Murray, J.D. Cashion, *Science* 298 (2002) 1762.
- [2] M.H. Zeng, M.X. Yao, H. Liang, W.X. Zhang, X.M. Chen, *Angew. Chem., Int. Ed.* 46 (2007) 1832.
- [3] M.Y. Li, B. Liu, B.W. Wang, Z.M. Wang, S. Gao, M. Kurmoo, *Dalton Trans.* 40 (2011) 6038.
- [4] M.D. Allendorf, C.A. Bauer, R.K. Bhakta, R.J.T. Houk, *Chem. Soc. Rev.* 38 (2009) 1330.
- [5] J. Cao, Y. Gao, Y. Wang, C. Du, Z. Liu, *Chem. Commun.* 49 (2013) 6897.
- [6] L.L. Liang, S.B. Ren, J. Zhang, Y.Z. Li, H.B. Du, X.Z. You, *Cryst. Growth Des.* 10 (2010) 1307.
- [7] L. Cheng, L.M. Zhang, S.H. Gou, Q.N. Cao, J.Q. Wang, L. Fang, *CrystEngComm* 14 (2012) 3888.
- [8] S. Perruchas, C. Tard, X.F. Le Goff, A. Fargues, A. Garcia, S. Kahlal, J.Y. Saillard, T. Gacoin, J.P. Boilot, *Inorg. Chem.* 50 (2011) 10682.
- [9] L. Zhang, Y. Ji, X. Xu, Z. Liu, J. Tang, *J. Lumin.* 132 (2012) 1906.
- [10] C. Schotes, M. Althaus, R. Aardoom, A. Mezzetti, *J. Am. Chem. Soc.* 134 (2012) 1331.
- [11] G. Ionescu, J.I. van der Vlugt, H.C.L. Abbenhuis, D. Vogt, *Tetrahedron: Asymmetry* 16 (2005) 3970.
- [12] T.L. Wang, L.G. Zhuo, Z.W. Li, F. Chen, Z.Y. Ding, Y.M. He, Q.H. Fan, J.F. Xiang, Z. X. Yu, A.S.C. Chan, *J. Am. Chem. Soc.* 133 (2011) 9878.
- [13] S. Nayak, H.P. Nayek, S. Dehnen, A.K. Powell, J. Reedijk, *Dalton Trans.* 40 (2011) 2699.
- [14] X. Yang, C. Chan, D. Lam, D. Schipper, J.M. Stanley, X. Chen, R.A. Jones, B.J. Holliday, W.K. Wong, S. Chen, Q. Chen, *Dalton Trans.* 41 (2012) 11449.
- [15] J. Long, F. Habib, P.-H. Lin, I. Korobkov, G. Enright, L. Ungur, W. Wernsdorfer, L. F. Chibotaru, M. Murugesu, *J. Am. Chem. Soc.* 133 (2011) 5319.
- [16] I.J. Hewitt, J.-K. Tang, N.T. Madhu, R. Clerac, G. Buth, C.E. Anson, A.K. Powell, *Chem. Commun.* (2006) 2650.
- [17] L.-L. Fan, F.-S. Guo, L. Yun, Z.-J. Lin, R. Herchel, J.-D. Leng, Y.-C. Ou, M.-L. Tong, *Dalton Trans.* 39 (2010) 1771.
- [18] Y. Deawati, D. Onggo, I. Mulyani, I. Hastiawan, D. Kurnia, P. Lönnecke, S. Schmorl, B. Kersting, E. Hey-Hawkins, *Inorg. Chim. Acta* 482 (2018) 353.
- [19] E. Molnár, B. Váradi, Z. Garda, R. Botár, F.K. Kálmán, É. Tóth, C. Platas-Iglesias, I. Tóth, E. Brücher, G. Tircsó, *Inorg. Chim. Acta* 472 (2018) 254.
- [20] N. Burkovskaya, G. Aleksandrov, E. Ugolkova, N. Efimov, I. Evstifeev, M. Kiskin, Z. Dobrokhotova, V. Minin, I. Eremenko, *New J. Chem.* 38 (2014) 1587.
- [21] J.-B. Tommasino, G. Chastanet, B.L. Guennic, V. Robert, G. Pilet, *New J. Chem.* 36 (2012) 2228.
- [22] A. Escuer, G. Aromí, *Eur. J. Inorg. Chem.* (2006) 4721.
- [23] X.-B. Li, Y. Ma, X.-M. Zhang, J.-Y. Zhang, E.-Q. Gao, *Eur. J. Inorg. Chem.* (2011) 4738.

- [24] T.-F. Liu, D. Fu, S. Gao, Y.-Z. Zhang, H.-L. Sun, G. Su, Y.-J. Liu, *J. Am. Chem. Soc.* 125 (2003) 13976.
- [25] L. Li, Z. Liu, S.S. Turner, D. Liao, Z. Jiang, S. Yan, *New J. Chem.* 27 (2003) 752.
- [26] G. Sheldrick, *Acta Crystallogr., Sect. A* 64 (2008) 112.
- [27] G.M. Sheldrick, *SADABS, The Siemens Area Detector Absorption Correction*, University of Göttingen, Göttingen, 2005.
- [28] B. Gole, K.C. Mondal, P.S. Mukherjee, *Inorg. Chim. Acta* 415 (2014) 151.
- [29] J.J. Borrás-Almenar, J.M. Clemente-Juan, E. Coronado, B.S. Tsukerblat, *J. Comput. Chem.* 22 (2001) 985.
- [30] Y. Song, G.N. Zhang, X.T. Qin, Y.F. Gao, S. Ding, Y.Q. Wang, C.F. Du, Z.L. Liu, *Dalton Trans.* 43 (2014) 3880.
- [31] D. Liu, Q. Zhou, Y. Chen, F. Yang, Y. Yu, Z. Shi, S.H. Feng, *Dalton Trans.* 39 (2010) 5504.
- [32] L.L. Cong, X.Y. Qin, W. Sun, Y.Q. Wang, S. Ding, Z.L. Liu, *New J. Chem.* 38 (2014) 545.
- [33] Y.-F. Zeng, X. Hu, F.-C. Liu, X.-H. Bu, *Chem. Soc. Rev.* 38 (2009) 469.